Thermal Fluorination and Annealing of Single-Wall Carbon Nanotubes

Pehr E. Pehrsson,*,† Wei Zhao,‡ Jeffrey W. Baldwin,† Chulho Song,‡ Jie Liu,§ Steven Kooi,†,|| and Bo Zheng§

Code 6174, Chemistry Division, Naval Research Laboratory, Washington, D.C. 20375, Department of Chemistry, University of Arkansas, Little Rock, Arkansas, and Department of Chemistry, Duke University, Durham, North Carolina

Received: October 17, 2002; In Final Form: March 3, 2003

Single-wall carbon nanotubes (SWNTs) were fluorinated with F_2 at 250 °C, and then some were heated under He to temperatures ranging from 100 to 400 °C to desorb the fluorine. The resulting samples were studied with X-ray photoelectron spectroscopy, Raman spectroscopy, IR spectroscopy, and electrical resistance measurements. The goals were to identify, as a function of fluorination and defluorination, the nature of the fluorine bonding, the damage to the tubes, the changes to the average tube diameter and proportions of metallic and semiconducting tubes, and the effects on the electrical conductivity and its mechanism. The stoichiometry of the as-fluorinated tubes was $CF_{0.43}$. Most of the time, F atoms bonded covalently to one carbon atom. Smaller amounts of CF_2 and CF_3 were probably bonded primarily at various defect sites. The fluorinated single-wall nanotubes were highly insulating. Upon heating, the largest fluorine loss occurred between 200 and 300 °C, and defluorination was virtually complete at 400 °C, but the largest resistance change occurred at 150−200 °C. Raman showed that both fluorination and thermal defluorination damaged the tubes by creating defects and/or amorphous carbon phases. Upon heating, most of the fluorinated SWNTs apparently reverted to SWNTs, rather than being etched. Thermal defluorination slightly increased the average tube diameter, but there was no Raman evidence of a change in the metallic/semiconducting tube ratio. However, the average length of tube bundles was substantially reduced. The resistance of the defluorinated SWNTs returned to that of the starting material, but a different conduction mechanism such as an amorphous carbon percolation network cannot be excluded.

Introduction

Fluorination is a chemical gateway to functionalization of single-wall carbon nanotube (SWNT) sidewalls.[1−4] It can also be used to modify their electronic properties,[5,6] enabling fabrication of metal/semiconductor junctions on a single tube, and for assembly of multicomponent structures consisting of multiple nanotubes or other nanostructures. Nanotubes are usually fluorinated thermally in F_2, with fluorination levels reaching 50%. Scanning tunneling microscopy (STM) of fluorinated single-wall nanotubes (FSWNTs)[8] revealed bonding along the tube sidewalls, which was attributed to partial, inhomogeneous fluorination of the sidewalls, and comprises possible evidence that fluorination initiates and spreads from specific sites such as defects.

It is unclear to what extent the aggressive fluorination and defluorination chemistries damage the tubes and, if so, whether the damage can be removed by thermal annealing under inert atmospheres.[7,8] (Hydrazine has also been used to defluorinate FSWNTs,[3] although Raman scattering shows that they also sustain damage.) A recent atomic force microscopy (AFM) study[9] revealed that FSWNTs were dramatically shortened by heating under Ar to 1000 °C. The authors suggested that the shortening may have occurred when the fluorinated regions etched during defluorination, leaving only the short, unfluorinated segments seen in the STM. This leaves unclear whether the etching occurred as the fluorine desorbed, or because the desorbing fluorine left highly defected nanotubes, which then disintegrated at higher temperatures.

In this paper, we examined SWNTs, which were fluorinated in F_2 at 250 °C and then annealed under He. The samples had been previously analyzed by some of the authors using UV−vis two-dimensional correlation spectroscopy.[7] The fluorinated and defluorinated samples were studied here with X-ray photoelectron spectroscopy (XPS), Raman spectroscopy, IR spectroscopy, AFM, and electrical resistance measurements. The goals were to characterize the fluorine bonding, the damage to the tubes, changes to the average tube diameter and proportions of metallic and semiconducting tubes, and the effects on the electrical conductivity and its mechanism.

Experimental Section

The procedure for preparing the nanotubes used in this study has been previously described.[7] Briefly, we used single-wall nanotubes (SWNTs) obtained from Tubes@Rice and grown by the laser vaporization method. The average diameter of the tubes was roughly 1.29 ± 0.05 nm, as confirmed by Raman scattering. The manufacturer acid-cleaned the tubes and annealed them under vacuum to 1000 °C. The acid treatment induces defects in the sidewalls, and leaves the edges of the defects terminated in carboxylic acids and other oxygen-containing groups.[10−12] The tubes were washed, filtered, and dried, and then fluorinated at 250 °C with a mixture of F_2 (20%) and N_2 (80%) in a Monel reactor (Parr Instrument). The total flow rate of the gas mixture

* Corresponding author. E-mail: Pehrsson@ccf.nrl.navy.mil.
† Naval Research Laboratory.
‡ University of Arkansas.
§ Duke University.
|| NRC/NRL Postdoctoral Fellow.

10.1021/jp027233s CCC: $25.00
Published on Web 05/24/2003

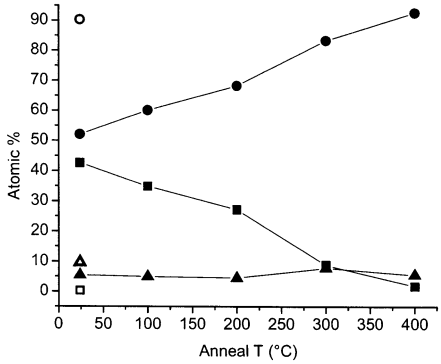

Figure 1. XPS-derived composition of unfluorinated (open symbols) and fluorinated and heated samples (closed symbols). Carbon is represented by circles, fluorine by squares, and oxygen by triangles.

TABLE 1: Sample Treatments and XPS-Derived Fluorine Atomic Concentration

sample	fluorination at 250 °C	anneal temp (°C)	at. % F
1	no	none	0
2	yes	none	43
3	yes	100	35
4	yes	200	27
5	yes	300	9
6	yes	400	2

was maintained at 30 sccm and reaction time was 10 h. Finally, the samples were heated in a tube furnace under flowing He, as shown in Table 1.

XPS of the fluorinated samples was performed in a Fisons Escalab 220-iXL spectrometer, using the monochromatized Al Kα line at 1486.6 eV. No charge correction was necessary for samples 1 and 4−6, but samples 2 and 3 had to be charge neutralized with an electron flood gun to compensate for the charge lost to the photoemission process. This energetically shifted the spectra, so the F 1s spectra of the charging samples were aligned with the F 1s peak in the uncompensated samples. The validity of this shift was checked by performing a peak fit on the C 1s region, which confirmed that the peak due to carbon sp^2 bonded with other carbon atoms was at the expected energy. The XPS data were analyzed with the Unifit software package, using an initial Tougaard background correction and peak fitting with mixed Gaussian/Lorentzian peaks. MicroRaman spectroscopy was performed on the samples using a Renishaw Raman spectrometer, with both 532 nm radiation (2.33 eV) from a frequency-doubled Nd:YAG laser and 488 nm radiation (2.54 eV) from an Ar laser. The spectra were calibrated with diamond single crystal and Si standards. The IR spectra were taken on a Nicolet NicPlan IR microscope, in the reflection mode, with a 50 μm spot size. The electrical properties of the films were analyzed using a two-point probe measurement with Au-coated "pogo" pins.

Finally, small portions of samples 1, 2, and 6 were placed in dimethylformamide and sonicated for 2 min. A drop of the resulting suspension was placed on Si coupons and imaged in air using an atomic force microscope (AFM).

Results

Figure 1 shows the XPS-derived composition of the unfluorinated nanotubes, the fluorinated nanotubes, and the fluorinated nanotubes after annealing under He to 100, 200, 300, or 400 °C. The composition of the fluorinated but otherwise unheated nanotubes was $\sim CF_{0.43}$, close to the presumed saturation stoichiometry of C_2F. The [F] dropped to ~35% after heating to 100 °C, but the biggest fluorine loss occurred after heating to 300 °C. After heating to 400 °C, there was only 2% fluorine, close to the detection limit. The oxygen level was about 9% before fluorination, consistent with other data we have observed, but dropped to 5% after fluorination. It increased again only slightly after heating to 300−400 °C.

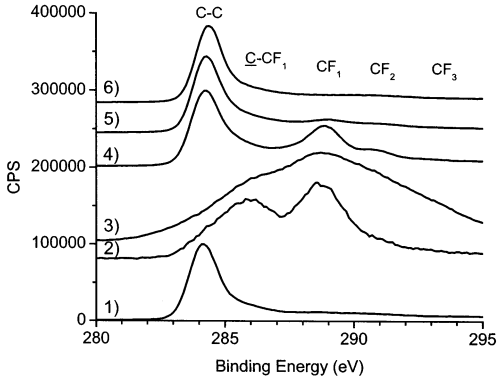

Figure 2. XPS C 1s spectra of fluorinated tubes. The spectra from the unannealed and 100 °C annealed samples were aligned with the 400 °C spectrum. The numbers associated with the traces are the same as the sample numbers in Table 1.

The XPS C 1s structures due to fluorinated carbons were tentatively assigned as shown in Figure 2, in agreement with similar peaks on fluorinated graphite,[13] carbon fibers,[14] amorphous carbon films,[15,16] nanoparticles,[13] fullerenes,[17] multiwall tubes,[18,19] and single-wall tubes.[20,21] Our fluorinated tubes exhibited two main peaks at 286.0 and 288.7 eV, which were attributed to a carbon bonded to monofluorinated carbon ($C-CF_1$) and carbon bonded to a single F atom (CF_1), respectively. These peaks were of roughly equal integrated intensity (53:47), consistent with the observed stoichiometry. The spectrum was virtually identical to that of graphite fluoride ($CF_{0.5}$).[13] A poorly resolved structure at higher binding energies was due at least in part to carbons bonded to multiple fluorine atoms. Annealing to 100 °C broadened the envelope of the peaks, but the most intense (albeit broad and poorly defined) peaks were at 286.4 and 288.6 eV, again corresponding to $C-CF_1$ and CF_1. Peak fitting revealed additional peaks at roughly 290.3 and 292.5 eV, which were assigned to CF_2, and CF_3, respectively. These latter species were assumed to be bonded primarily at defects and edges such as open tube ends. Heating to 200 °C more clearly defined the CF_1 and CF_2 peaks at 289.0 ± 0.3 and 290.5 ± 0.2 eV. At 300 °C, the F-induced peaks were much smaller, reflecting the reduced fluorine concentration. The peaks for multiply fluorinated carbon were essentially gone. Such instability is consistent with carbon atoms bonded at the tube edges. Edge-bonded carbons need break only one or two C−C bonds to desorb from the tube while a carbon with a single C−F bond would have to break three C−C bonds to desorb. The 400 °C spectrum was very similar to that of the starting material.

As previously noted, the spectra of samples 2 and 3 were shifted due to sample charging. Such charging was expected given the electrical resistance measurements, which increased by $\sim 10^7$ upon fluorination (Figure 3). The samples annealed to 200 °C or higher did not need charge neutralization, consistent with the large drop in the resistance back to the level of the unfluorinated tubes.

Figure 4 shows the difference spectrum for the inelastic loss region from the C 1s spectra of unfluorinated tubes (sample 1) and fluorinated tubes after heating to 400 °C (sample 6). The main C−C peaks were normalized to the same intensity, and the peak maxima were aligned. There were three main com-

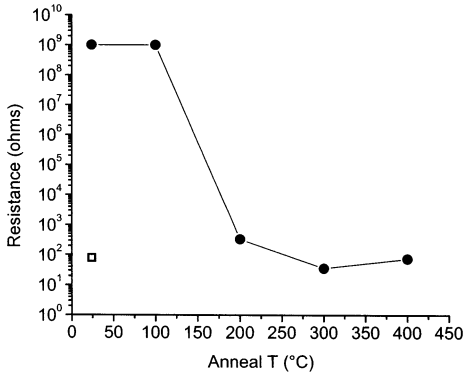

Figure 3. Resistance vs anneal temperature of fluorinated nanotubes. The unfluorinated tubes are represented by the open square, and the closed circles are the fluorinated tubes heated to the indicated temperature. The measurements were made in a two-point probe apparatus, but resemble previous measurements made with a four-point probe apparatus.[7]

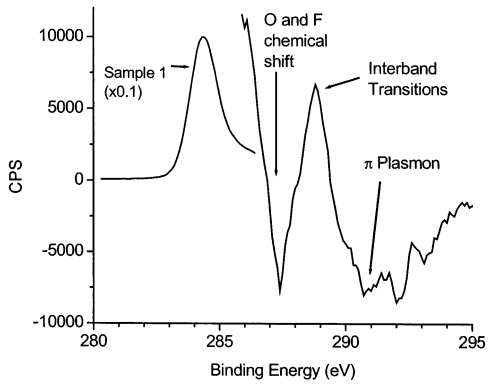

Figure 4. Difference spectrum of the C 1s inelastic loss region for unfluorinated sample (sample 1) minus fluorinated sample heated to 400 °C (sample 6).

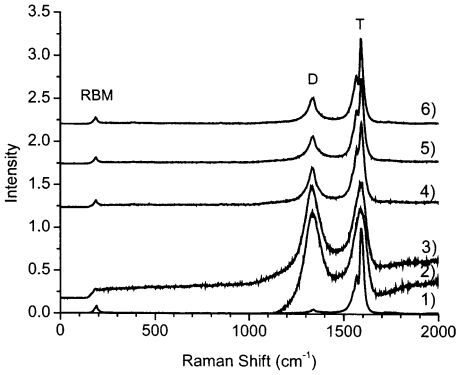

Figure 5. Raman spectra of samples shown in Figures 1 and 2. The wavelength of the exciting laser was 532 nm. The spectra were normalized using the main tangential mode at 1591 ± 1 cm^{-1}. The traces are numbered as in Figure 2.

ponents in this inelastic loss region. The minimum which peaked at 3 eV from the main C 1s peak is attributed to oxygen and residual fluorine-induced features after defluorination.[13−21] The peak at 4.4 eV is due to interband transitions, and the broad minimum at about 6 eV corresponds to the graphitic or amorphous carbon π-plasmon. The development of this latter feature supports the conclusion from the Raman data that the annealed nanotubes contain more defects or nontube sp^2 carbon than the starting material.

Figure 5 shows Raman spectra from the same samples shown in Figures 1−3. Three main regions reveal the nanotube bonding

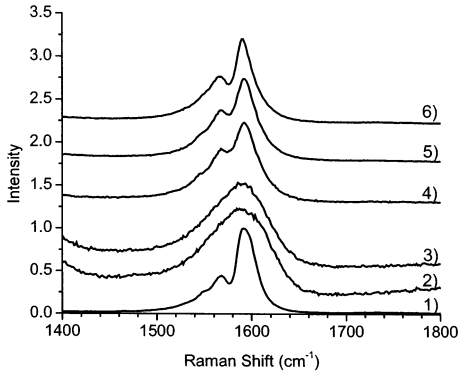

Figure 6. Expanded view of Figure 5 showing tangential modes of various fluorinated nanotubes. The wavelength of the exciting laser was 532 nm. The traces are numbered as in Figure 2.

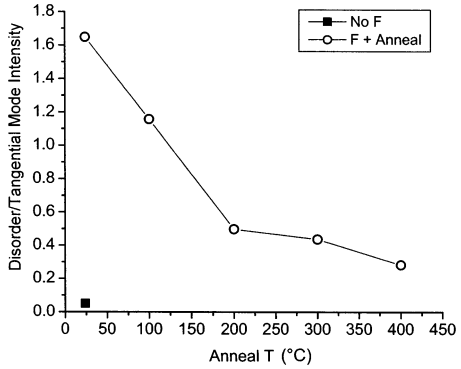

Figure 7. Changes in the ratio of the Raman disorder mode at 1337 ± 4 cm^{-1} to the tangential mode at 1591 ± 1 cm^{-1} upon fluorination and annealing. The black square is the starting material (sample 1), and the open circles are samples 2−6 after fluorination and heating.

and structure: the main radial breathing mode (RBM) at 189 cm^{-1}, the tangential modes at 1500−1620 cm^{-1}, and the disorder (D) mode at 1337 ± 4 cm^{-1}, which is attributed to nanocrystalline graphite,[22] amorphous carbon, and defected or damaged nanotubes.[23] Sample 1 had the Raman features expected of high-quality, single-wall nanotubes, especially the low disorder mode peak and a main tangential mode at 1592 cm^{-1}. A published conversion factor ($\omega_r = 223.75$ (cm^{-1} nm)/d_t (nm) + $\Delta\omega_g$ cm^{-1}, where $\Delta\omega_g = 16$) based on TEM and AFM measurements of tube dimensions for bundled tubes indicates that the average tube diameter was ∼1.3 nm.[24]

Fluorination broadened the separate tangential modes (Figure 6) into one very broad, but still intense peak at roughly 1590 cm^{-1}. The distinct tangential modes reappeared after the 200 °C anneal. The energy of the main peak was little changed at 1591 cm^{-1}, and the relative intensities of the different contributions to the peaks were similar to those of the starting material.

The Raman D mode greatly increased after fluorination, but was sequentially reduced after heating to higher temperatures. Figure 7 shows that the ratio of the D mode to the main tangential mode never fully returned to its low initial value even after virtually all of the fluorine had desorbed at 400 °C. Figure 8 shows that fluorination also virtually eliminated the RBM, and downshifted what little intensity remained to 177 cm^{-1}. The RBM intensified upon heating to ≥200 °C, but remained downshifted, indicating that the remaining tubes had a slightly larger average diameter (∼1.4 nm) than the starting material. This result probably reflects selective etching of the smallest diameter tubes, since smaller tubes are more highly strained, and thus have less stable C−C bonds.[25,26]

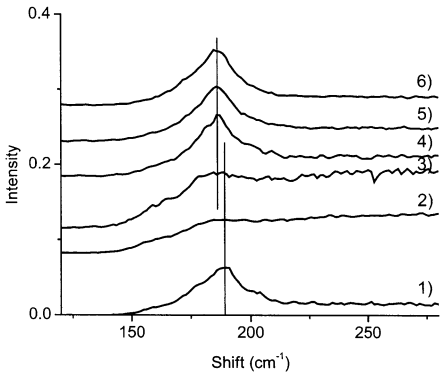

Figure 8. Expanded view of Figure 5 showing radial breathing modes of various fluorinated nanotubes. The wavelength of the exciting laser was 532 nm. The traces are numbered as in Figure 2.

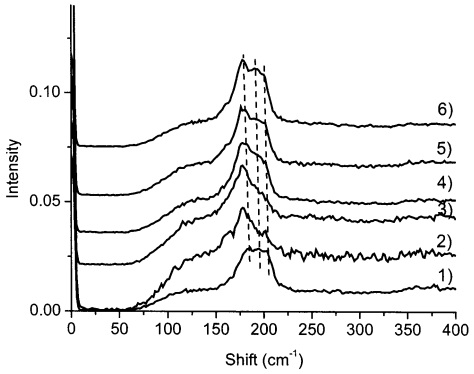

Figure 9. Radial breathing modes of fluorinated nanotubes. The wavelength of the exciting laser was 488 nm. The traces are numbered as in Figure 2.

Figure 9 shows the 184 and 204 cm^{-1} radial breathing modes of the various tubes obtained using a 488 nm laser source. The main peak for both sources was downshifted by 4−6 cm^{-1} upon fluorination and annealing, again indicating a slight increase in the average tube diameter.

Infrared Spectroscopy. The IR spectra of our samples (not shown) had a main ν(C−F) peak at 1260 cm^{-1}, with a shoulder at 1217 cm^{-1} and a very small feature at about 1175 cm^{-1}. Heating to 200 °C and above shifted the (now reduced) main peak to 1280 cm^{-1} and generated a small peak at 1183 cm^{-1}. A previous paper[7] showed similar values at 1270 and 1184 cm^{-1} prior to heating, and 1278, 1216, and 1188 cm^{-1} after heating to 350 °C.

AFM. Sample 1 appeared normal, consisting of microns-long isolated tube bundles. Sample 2 consisted of many intertwined tube bundles, which made it difficult to ascertain their length. Sample 6 was radically different, consisting mostly of short (hundreds of nanometers) isolated sections, similar in appearance to published pictures[9] of tubes annealed to 1000 °C.

Discussion

Fluorination. There is a division in the fluorination conditions above which the SWNTs are destroyed due to the formation of more C−F bonds and further breaking of the C−C bonds. SWNTs have been shown to disintegrate at 350 °C, while fluorination at 250 °C for 5 h produces more optimal material.[4] In addition, XPS also suggests that fluorination temperatures below 200 °C result in semi-ionic C−F bonds but covalent sp^3 bonds at higher temperatures.[20] Other workers put the dividing line between semi-ionic and covalent bonding at about 150 °C.[4]

The combination of XPS and Raman spectroscopies with resistance measurements and the previous UV−vis results provides a detailed picture of the fluorination products and the defluorination process at different temperatures. XPS showed that the stoichiometry of our tubes was about C_2F; i.e., the tubes were fully fluorinated. The fluorine was covalently bonded, primarily as CF_1 with a binding energy of 288.7 ± 0.3 eV. This value is higher than those attributed to semi-ionically bonded fluorine seen with some intercalated graphite[14] or SWNTs[20] at lower fluorination temperatures and coverages. The region to the high binding energy side of the main C 1s XPS peak contains inelastic loss modes[27] and chemically shifted peaks derived from carbon bonded in various ways to fluorine.[18] As noted above, there are smaller CF_2 and CF_3 peaks at 290.3 and 292.5 eV. The relative distribution of these species changes with postfluorination heating, especially between 100 and 200 °C. The 100 °C sample (sample 3) had large CF_2 and CF_3 contributions, which were much smaller on the unheated sample (sample 2) and are smaller again on sample 4. However, it is difficult to unequivocally assign intensity in this region since there are also contributions from the nanotube $\pi\pi^*$ plasmon and interband transitions.[27,28] The analysis is further complicated by the amorphous and graphitic carbon, which can contaminate even purified single-wall nanotube material. Thus, there are potential XPS C 1s inelastic loss contributors in the 4.5−5.5 eV range from the nanotubes[27] and 5−6.5 eV from amorphous carbon and/or graphitic carbon contaminants.

The F 1s binding energy of our fibers heated to ≥200 °C was 687.8 ± 0.3 eV, virtually identical to the 687.7 ± 0.3 eV observed for fluorine covalently bonded to the outside of carbon fibers.[14] The uncertainty associated with absolute binding energies on the charging samples was removed by using the C 1s and F 1s peak separation as a metric, although a chemically based change in the F 1s energy is a possible complication. The F 1s peak was separated from the CF_1 peak by 398.7 eV on sample 2 and 398 eV on sample 3. Sample 4, which did not charge, had a 398.7 eV separation. Other workers report that covalently bonded fibers had a value of 399.2 eV.[14]

The IR ν(C−F) frequency of 1260 cm^{-1} that we observed is consistent with literature values for covalently bonded fluorine. Some fluorination conditions, typically lower temperature and F_2 concentration, generate related systems such as graphite-intercalated compounds in which the fluorine forms a semi-ionic bond to the carbon[14] and has a lower ν(C−F) than with covalently bonded fluorine. For example, the ν(C−F) feature in laser-grown SWNTs[4] shifted from 1201 to 1176 cm^{-1} when the fluorination temperature was reduced from 250 to 200 °C. Likewise, SWNTs fluorinated at 50 °C had a stoichiometry of $CF_{0.2}$ and had ν(C−F) peaks at 1111 and 1221 cm^{-1}, which were assigned to semicovalent and covalent C−F, respectively.[9] Multiwall nanotubes fluorinated at room temperature in a mixture of F_2 and HF had a broad ν(C−F) mode at 1100 cm^{-1} which was attributed to semi-ionic C−F bonds.[29] When the same nanotubes were fluorinated at 500 °C in pure F_2, ν(C−F) narrowed and shifted to 1220 cm^{-1}, and was attributed to covalent C−F.

The changes in the Raman spectra (disappearance of the radial breathing mode and the individual tangential modes, and the enhancement of the disorder mode) have been observed with nanotubes fluorinated by others.[2,3,4,9] The increase in the D mode can be attributed to defects, amorphous carbon, nanocrystalline graphite, and possibly very short nanotubes, but the exact cause for the fluorinated SWNTs remains unclear. The reason for the changes to the other modes is unknown, but the reduction in

the radial breathing mode is consistent with selective etching of smaller tubes. In addition, increased tube spacing may reduce the value of $\Delta\omega_g$ and hence the RBM frequency and apparent tube diameter. There may also be changes in the intertube spacing due to the fluorine on the tube sidewalls. Changes in the tube−tube interactions were identified as the cause of an upshift in the RBM frequency of isolated tubes in solution compared to those in large solid bundles.[24] There was little effect on the tangential mode frequency, similar to the result we observed. Since doping moves both the RBM and the tangential mode,[23] our observations are consistent with a change in the intertube interactions caused by a change in the tube−tube spacing due to fluorine on the SWNT walls. X-ray diffraction and TEM were used to demonstrate the loss of crystallinity and changes in the layer spacing in multiwall carbon nanotubes fluorinated under conditions similar to ours.[29]

Fluorination increased the resistance of our films by 10^7. Increased tube−tube spacing due to the fluorine presumably lowers tube to tube electron transmission since few tubes are long enough to span the distance between the contacts and a carrier must therefore move from tube to tube to cross the interprobe distance. Fluorination decreases the electrical conductivity of any one tube by disrupting its π conjugation, as evidenced by the featureless UV−NIR spectra.[1] Similar large changes have been observed on fluorinated amorphous carbon (a-C:F) films[16,30] as well as graphite fibers intercalated with F.[31] The latter paper notes that C_xF fibers undergo a transition from a weakly localized electronic system when $x > 0.36$ to a strongly localized system when $x < 0.36$, where x is the carbon-to-fluorine ratio. In contrast, the conductivity of graphite-intercalated compounds (GICs) and SWNTs[32] usually increases with doping.

The apparent reduction in bundle and/or tube length does not necessarily indicate that the individual tubes are shortened by defluorination. Tubes with fluorine, amorphous carbon, or defects and associated oxygen on the sidewalls would be expected to exhibit less proclivity to form bundles. A more carefully controlled AFM investigation of these tubes is underway to determine the exact nature of the material after each heat treatment and whether most of the tubes are destroyed or restored.

Although not directly comparable, the low resistivity of the previously mentioned SWNTs fluorinated at 50 °C[20] indicates that they were more conductive than our FSWNTs. More importantly, the maximum fluorination-induced resistivity change at any temperature was less than 100×, while fluorination increased the resistance of our samples by 10^5−10^7. However, this other work[20] mentioned no cleaning steps to remove the catalyst and amorphous carbon, so conduction through metals or amorphous carbon cannot be excluded. Residual metal catalyst and amorphous carbon contamination can greatly affect nanotube chemistry,[33] so useful comparisons of SWNT fluorination require that the catalyst be removed and the tubes then be annealed to remove any cleaning-induced damage. Our material was acid-cleaned and heated to 1000 °C in a vacuum, and we did not detect metal catalyst with XPS, although TEM revealed that some catalyst was still present. Raman showed that the amorphous carbon contamination was low in the starting material.

Taken together, these data indicate that the fluorine on the tubes bonds covalently, primarily as CF_1, in agreement with most theoretical studies of both armchair (10,0) and zigzag (10,0 or 18,0) tubes.[6,8,34−36] The conductivity of the fluorinated tubes depends on whether the fluorinated carbon atoms, and hence the π bonds on the unfluorinated carbon atoms, form continuous chains along the tube axis.[34] Most studies predict that fluorinated tubes are semiconducting or insulating, except when a continuous π-bonded chain runs along the tube axis, rendering the tube metallic. The reduction we observed in the conductivity of the tube mat and the previously reported banding around the circumference of the tubes[8] suggests that at least a significant part of the tubes are bonded in rows with isolated C═C bonds normal to the tube axis (the 1,4 configuration for armchair tubes[8]).

Defluorination. The changes in the amount and type of F bonding with postfluorination heating are correlated with, but not identical to, the changes in resistance. Figure 1 shows that the [F] dropped fast (to about 10%) from 200 to 300 °C. Therefore, adsorption, desorption, and some etching probably occur simultaneously during the fluorination process at 250 °C. More easily desorbed reaction products that are present on tubes fluorinated at lower temperatures will presumably be desorbed and thus absent from our material.

The slight shift of the main C−C peak to about 284.4 eV is consistent with formation of at least some sp^3 nontube carbon.[20,16] Meanwhile, the $C-CF_1$, CF_1, CF_2, and CF_3 XPS peaks disappeared as the overall fluorine concentration dropped. The inelastic loss region is similar for samples 1 and 6, indicating that the material heated to 400 °C was largely the same as on the unfluorinated tubes. The main differences highlighted in Figure 4 show higher amounts of oxygen or residual fluorine covalently bonded to the tubes after fluorination, and to the more intense plasmon at 6 eV and higher. A higher concentration of amorphous carbon or graphite from the defluorination could cause such a result, since pure SWNTs have a lower plasmon energy.[27,28] The loose inverse proportionality between the oxygen and fluorine concentrations is presumably due to the blocking of reactive radical sites by one or the other, as was also observed for a-C:F films.[16] However, the absence of dramatically higher oxygen levels at 400 °C is also consistent with tubes in which much of the reactive, damaged carbon has been annealed.

The reappearance of the Raman radial breathing and tangential modes and the reduction of the disorder mode coincide with the loss of the fluorine in the XPS, and show that at least part of the tubes remain after fluorination and defluorination. Figure 7 shows that the disorder mode does not return to its initial low relative intensity upon defluorination. It is unclear if most of the fluorinated tubes recovered to their original state by desorbing their fluorine or if the Raman spectrum recovered because the fluorinated material was etched away, as suggested by our own results as well as other observations of extreme tube shortening during thermal defluorination.[9] The latter interpretation is consistent with suggestions that the disorder mode is strongest for short tubes, i.e., that the tube ends are the defects responsible for this feature.[23]

As discussed below, the Raman spectra provide some information on the ratio of the metallic to semiconducting tubes, which according to the manufacturer normally occur in a roughly 1:2 ratio. It has been suggested that the highly fluorinated parts of the tubes etch upon defluorination,[9] leaving short fragments. Such etching might shift the distribution of the tubes if one tube type etches more readily. The envelope of the Raman tangential modes, shown in expanded view in Figure 6, was fitted with peaks at 1590, 1565, 1545, and 1450 cm^{-1}. The peaks at about 1590 and 1545 cm^{-1} peaks (depending on the excitation wavelength used) are associated with semiconducting and metallic tubes respectively[23] and can indicate changes in the

ratio of the two tube types as a result of selective etching. A peak fit of the postanneal tangential modes reveals only minor changes from the starting material, indicating that the metallic to semiconducting tube ratio was largely unchanged, confirming the conclusion reached in a previous paper[7] using UV−vis spectroscopy. A longer wavelength laser source would have been preferable, to resonantly enhance the Raman signal from the metallic tubes. Access to such capacity is being sought.

It is unclear whether the fluorine desorbs directly as fluorine atoms or a fluorocarbon fragment, recombines on the surface and desorbs as F_2, or reacts with other ambient species such as oxygen or hydrogen. Elucidation of the mechanism will require scrupulous control of oxygen and hydrogen, and of metal nanoparticle contamination. A recent thermogravimetric analysis (TGA) study[9] of SWNTs fluorinated at 50 °C showed that the primary desorption products (CO_2 and COF_2) desorbed at 300−560 °C, followed by CF_4 at >560 °C. Yet most of the fluorine on our tubes had already been lost at those temperatures.

The resistance of the material heated to 200 °C and above recovers to the unfluorinated level. The measurements from a previous paper[7] included a sample heated to 150 °C, and showed that the resistance had largely recovered to its value in the untreated tubes at that point. However, the conduction mechanism may not be the same. For example, the Raman results suggest that the enhanced disorder mode could reflect a higher concentration of amorphous carbon, perhaps enough to form a percolation network for electrical conduction.

Conclusions

The tubes fluorinated at 250 °C have a $CF_{0.43}$ stoichiometry, close to full fluorination without destroying the tubes. Most of the F is covalently bonded to a single carbon atom, with smaller amounts of CF_2 and CF_3. The bonding is not the semi-ionic type seen with intercalated graphite at lower fluorination temperatures and coverages, so the FSWNTs are highly insulating. Thermal defluorination is virtually complete at 400 °C. The largest drop in electrical resistance occurs at 150−200 °C, whereas most of the fluorine desorbs from 200 to 300 °C. Both fluorination and thermal defluorination create some defects and possibly amorphous carbon phases. Thermal defluorination slightly reduces the average tube diameter, but there is no evidence of a change in the metallic/semiconducting tube ratio. The resistance of the defluorinated SWNTs reverts to that of the unfluorinated material, but a different conduction mechanism, e.g., percolation through amorphous carbon, may be responsible.

Acknowledgment. The authors thank ONR (P.E.P.) and ARO under Award No. DAAD 190210140 (W.Z.) for financial support, Robert Mowrey for assistance with IR measurements, and Jim Butler for assistance with Raman measurements. The work at Duke was in part supported by a grant from NASA (NAG-1-01061) through a subcontract from the University of North Carolina.

References and Notes

(1) Boul, P. J.; Liu, J.; Mickelson, E. T.; Huffman, C. B.; Ericson, L. M.; Chiang, I. W.; Smith, K. A.; Colbert, D. T.; Hauge, R. H.; Margrave, J. L.; Smalley, R. E. *Chem. Phys. Lett*. **1999**, *310*, 367.

(2) Mickelson, J. *Chem. Phys. Lett*. **1998**, *296*, 188.

(3) Mickelson, J. *J. Phys. Chem. B* **1999**, *103*, 4318.

(4) Chiang, I. Ph.D. Dissertation, Rice University, 2001.

(5) Braier, N. C.; Jishi, R. A.; Mintmire, J. W.; White, C. T. Unpublished results.

(6) Seifert, G.; Kohler, T.; Frauenheim, T. *Appl. Phys. Lett*. **2000**, *77*, 1313.

(7) Zhao, W. Song, C.; Zheng, B.; Liu, J.; Viswanathan, T. *J. Phys. Chem. B* **2002**, *106*, 293.

(8) Kelly, K. F.; Chiang, I. W.; Mickelson, E. T.; Hauge, R. H.; Margrave, J. L.; Wang, X.; Scuseria, G. E.; Radloff, C.; Halas, N. J. *Chem. Phys. Lett*. **1999**, *313*, 445.

(9) Gu, Z.; Hauge, R. H.; Smalley, R. E.; Margrave, J. L. *Nanoletters* **2002**, *2*, 1009.

(10) Kuznetsova, A.; Yates, J. T., Jr.; Simonyan, V. V.; Johnson, J. K.; Huffman, C. B.; Smalley, R. E. *J. Chem. Phys.* **2001**, *115*, 6691.

(11) Zhao, W.; Song, C.; Pehrsson, P. E. *J. Am. Chem. Soc*. **2002**, *124*, 12418.

(12) Yang, Y.; Zhang, J.; Nan, X.; Liu, Z. *J. Phys. Chem. B* **2002**, *106*, 4139.

(13) Okotrub, A. V.; Yudanov, N. F.; Chuvilin, A. L.; Asanov, I. P.; Shubin, Yu. V.; Bulusheva, L. G.; Guselnikov, A. V.; Fyodorov, I. S. *Chem. Phys. Lett.* **2000**, *322*, 231.

(14) Tressaud, A.; Guimon, C.; Gupta, V.; Moguet, F. *Mater. Sci. Eng. B* **1995**, *30*, 61.

(15) Wijesundara, M. B. J.; Ji, Y.; Ni, B.; Sinnott, S. B.; Hanley, L. *J. Appl. Phys*. **2000**, *88*, 5004.

(16) Leezenberg, P. B.; Johnston, W. H.; Tyndall, G. W. *J. Appl. Phys.* **2001**, *89*, 3498.

(17) Bulusheva, L. G.; Okotrub, A. V.; Yudanov, N. F. *J. Phys. Chem. A* **1997**, *101*, 10018.

(18) Ni, B.; Andrews, R.; Jacques, D.; Qian, D.; Wijesundara, M. B. J.; Choi, Y.; Hanley, L.; Sinnott, S. B. *J. Phys. Chem. B* **2001**, *105*, 12719.

(19) Ago, H.; Kugler, T.; Cacialli, F.; Salaneck, R. W.; Shaffer, M. S. P.; Windle, A. H.; Friend, R. H. *J. Phys. Chem. B* **1999**, *116*, 8116.

(20) An, K.; Heo, J. G.; Jeon, K. G.; Bae, D. J.; Jo, C.; Yang, C. W.; Park, C.-Y.; Lee, Y. H.; Lee, Y. S.; Chung, Y. S. *Appl. Phys. Lett*. **2002**, *80*, 4235.

(21) Lee, W. H.; Kim, S. J.; Lee, W. J.; Lee, J. G.; Haddon, R. C.; Reucroft, P. J. *Appl. Surf. Sci*. **2001**, *181*, 121.

(22) Solin, S. A.; Nemanich, R. J. *Phys. Rev. B* **1979**, *20*, 392.

(23) Dresselhaus, M. S.; Eklund, P. C. *Adv. Phys*. **2001**, *49*, 705.

(24) Rao, A. M.; Chen, J.; Richter, E.; Schlecht, U.; Eklund, P. C.; Haddon, R. C.; Venkateswaran, U. D.; Kwon, Y.-K.; Tománek, D. *Phys. Rev. Lett*. **2001**, *86*, 3895.

(25) Yang, Y.; Zou, H.; Wu, B.; Li, Q.; Zhang, J.; Liu, Z.; Guo, X.; Du, Z. *J. Phys. Chem. B* **2002**, *106*, 7160.

(26) Srivastava, D.; Brenner, D. W.; Schall, J. D.; Ausman, K. D.; Yu, M.; Ruoff, R. S. *J. Phys. Chem. B* **1999**, *103*, 4330.

(27) Reed, B. W.; Sarikaya, M. *Phys. Rev. B* **2001**, *64*, 195404.

(28) Pichler, T.; Knupfer, M.; Golden, M. S.; Fink, J. Rinzler, A.; Smalley, R. E. *Phys. Rev. Lett*. **1998**, *80*, 4729.

(29) Hamwi, A.; Alvergnat, H.; Bonnamy, S.; Beguin, B. *Carbon* **1997**, *35*, 723.

(30) Biswas, N.; Harris, H. R.; Wang, X.; Celebi, G.; Temkin, H.; Gangopadhyay, S. *J. Appl. Phys*. **2001**, *89*, 4417.

(31) Rao, A. M.; Fung, A. W. P.; di Vittorio, S. L.; Dresselhaus, M. S.; Dresselhaus, G.; Endo, M.; Oshida, K.; Nakajima, T. *Phys. Rev. B* **1992**, *45*, 6883.

(32) Lee, R. S.; Kim, H. J.; Fischer, J. E.; Thess, A.; Smalley, R. E. *Nature* **1997**, *388*, 255.

(33) Chiang, I. W.; Brinson, B. E.; Smalley, R. E.; Margrave, J. L.; Hauge, R. H. *J. Phys. Chem. B* **2001**, *105*, 1157.

(34) Kudin, K. N.; Bettinger, H. F.; Scuseria, G. E. *Phys. Rev. B* **2001**, *63*, 045413.

(35) Bauschlicher, C. W. *Chem. Phys. Lett*. **2000**, *322*, 237.

(36) Khabashesku, V. N.; Billups, W. E.; Margrave, J. L. *Acc. Chem. Res*. **2002**, *35*, 1087.